Summer 7-27-2023

Examining Protein Localization via Fluorescence Microscopy in Saccharomyces cerevisiae

Lewis Barr
lewis.barr@bobcats.gcsu.edu

Richard H. Adams
University of Arkansas

Ellen France PhD
Georgia College & State University

Examining Protein Localization via Fluorescence Microscopy in *Saccharomyces cerevisiae*

Lewis Barr

A THESIS

Submitted to Georgia College and State University

In partial fulfillment of the requirements

For the degree of

Master of Science

Dr. Ellen France, Faculty Advisor

Department of Biological and Environmental Sciences

Milledgeville, GA

July 2023

Georgia College & State University

College of Arts and Sciences

Department of Biological and Environmental Sciences

We hereby approve the thesis of

Examining Protein Localization via Fluorescence Microscopy in *Saccharomyces cerevisiae*

Lewis Barr

Candidate for the degree of Master of Science

_____	_____
Dr. Ellen France Major Professor	Date
_____	_____
Dr. Ashok Hegde Committee Member	Date
_____	_____
Dr. Richard Adams Committee Member	Date
_____	_____
Dr. Eric Tenbus Dean of College of Arts and Sciences	Date

Acknowledgments

I would like to express my gratitude towards Georgia College and State University Department of Biological and Environmental Sciences for their continued support throughout my education. I want to thank my committee members Dr. Ashok Hegde and Dr. Richard Adams for their suggestions and guidance during my project. I would also like to extend my thanks to the faculty and staff in the Department of Biological and Environmental Sciences for their willingness to help and teach me. To the HKS, especially Molly Bullington, Sophia McNeill, Ivan Chu, and Kai Spetalick, thank you for giving me an extra hand when experiments became overwhelming. Thank you to my friends and family for their unwavering support and optimism. Once more, I would like to thank Dr. Ellen France for constantly believing in my abilities and pushing me to achieve my goals. Thank you for your infinite words of wisdom and your efforts to prepare me for my future in academia.

Table of Contents

List of Tables

List of Figures

Abstract

Twenty-seven years ago, *Saccharomyces cerevisiae* became the first eukaryote to have its full genome sequenced, thus leading to the discovery that 30% of genes related to human diseases are orthologous to those in *S. cerevisiae*. Since then, 75% of the proteome has had its localization classified, and we sought to fill the remaining gaps of knowledge by identifying the localization of three proteins: Fsh3, Gid10, and Ade13, which function as a serine hydrolase, ubiquitin ligase, and adenylosuccinate lyase, respectively. To visualize cellular localization, we used a C-terminal GFP tagging strategy and subsequent fluorescence microscopy. Through colocalization analyses, we identified the cellular localization of Ade13 to be mitochondrial while Fsh3 and Gid10 localize to distinct puncta which are predicted to be peroxisomal. Interestingly, we observed that the localization of Gid10 changes depending on the glucose availability in the media. As each investigated yeast protein has human orthologues whose malfunctions lead to diseases in humans, our findings lay important basic foundations for future studies comparing *S. cerevisiae* and human proteins in conserved processes.

Introduction

Overview of *Saccharomyces cerevisiae*

Saccharomyces cerevisiae is a unicellular organism that belongs to the Fungal phyla Ascomycota. Fungi are predominantly heterotrophs and fall into the category of decomposers via the oxidation of carbon-based molecules to carbon dioxide (Wisecaver et al. 2014). The carbon substrate that fungi target can range from organic polymers such as cellulose and lignin to simple sugars like glucose (Wainright 1988). Specifically, *S. cerevisiae* exhibits a unique metabolic niche targeting simple sugars through what is known as the Crabtree effect which describes the aerobic fermentation of sugars to produce ethanol and carbon dioxide (Crabtree 1929). The unique metabolic capabilities of natural *S. cerevisiae* enable it to flourish in harsh competitive microbial environments (De Deken 1966). This advantageous trait also helped carve a niche in the development of mankind as ethanol and carbon dioxide production have been used by humans to brew and bake since early civilizations, hence reflected in its nickname, "Baker's yeast". The initial spread of the organism can be tracked from 7000 BC China across the silk road to Egypt in 3000 BC (Lahue et al. 2020). Domesticated lineages of *S. cerevisiae* are not well understood, and it was not until 2018 that two major groups of these lineages were identified to originate from China (Duan et al. 2018).

For thousands of years, *S. cerevisiae* was only used for baking and brewing, and humans simply took advantage of the favorable commodities produced by the organism without knowing why or how. It was not until 1857 that Louis Pasteur discovered alcoholic fermentation. As a result, research efforts were established to optimize brewing and better understand *S. cerevisiae* as an organism (Liti 2015). In the laboratory, *S. cerevisiae* was quickly established as a key eukaryotic model organism. It obtained this moniker because of three fundamental qualities. One reason is

that it is a simple organism to maintain and store (Duina et al. 2014). *S. cerevisiae* daughter cells pinch off mother cells dividing every 90 minutes through a process known as budding, giving them the name 'budding yeast'. Lacking the need for an incubator, cells are easily maintained through growth on agar plates at room temperature. Furthermore, stocks can be kept through freezing in 10% glycerol and stored at -80°C. Apart from its relative ease to maintain and grow in laboratory conditions, *S. cerevisiae* is considered to be a model organism due to its comparative abilities associated with humans. Second, *S. cerevisiae* can exist as a stable haploid or diploid cell (Dickinson and Schweizer 2004.) The experimentation of single genes allows for mutations to reveal phenotypes in haploid states without the complications of heterozygous genes. Finally, 30% of genes related to human diseases are considered orthologs between the two species (Karathia et al. 2011). These elements have allowed *S. cerevisiae* to become an important eukaryotic model system for cellular and molecular research.

Due to the importance of *S. cerevisiae* as a model organism in genomic research, a singular strain (S288c) was created by Mortimer and Johnston in 1985 as a reference for genomic and proteomic work with the organism. In 1996, S288c became the first eukaryotic organism to ever have its genome fully sequenced (Goffeau et al. 1996). In this study, 5885 potential protein-encoding genes were identified across 12.068 megabases and 16 chromosomes. Sequencing of the entire genome required the implementation of a database for the storage of this information, and in 1998, the *Saccharomyces* Genome Database was created for internet access to the genome and *S. cerevisiae* based research. The establishment of the database subsequently generated a multitude of genome and proteome-wide discoveries, which still actively continues today. In 2002, the *S. cerevisiae* Deletion Project by Giaever et al. created 21,000 mutants containing ~6,000 open reading frame deletions, which made *S. cerevisiae* the first organism with a systematically created

deletion collection. Through this project, 18.7% of Open Reading Frames (ORFs) were determined to be essential for growth. 'Essential' means that upon deletion of the gene, the cell would lose viability. Next, Sopko et al. (2002) utilized the loss-of-function approach to explore the effect of gene overexpression. In this project, genes were overexpressed, and the growth rate of these strains was analyzed. Through the assessment of over 80% (5,280 genes) of the genome, 15% (769) of overexpression strains showed a decrease in growth rate.

Cellular and molecular investigation of S. *cerevisiae* has maintained itself as an incredibly important task due to its fundamental qualities as a model organism, and efforts to describe the yeast genome via large-scale studies have been a major outlet for investigation. Adding to the growing knowledge regarding *S. cerevisiae,* was the analysis of protein localization by a large consortium (Huh et al. 2003). The primary method for the study was via a high throughput GFP-tagging of each protein (a total of 6,029) in the proteome followed by the fluorescence-based localization of 75% (4,156 proteins) of the yeast proteome. By identifying the localization of proteins, their function in relation to their environment can be better understood. The landmark project pursued by Huh et al. however, still left 25% of the proteins with unknown localization and therefore a significant number of proteins are still to be examined for their cellular localization.

For this study, we chose three such proteins for localization analysis: Ade13, Gid10, and Fsh3. Each protein was chosen because orthologs of these proteins appeared to play important roles in higher eukaryotes including humans, and their localization was yet to be reported in *S. cerevisiae.* In addition to a lack of localization knowledge, these three chosen proteins are associated with human diseases upon mutation of their human orthologs.

Ade13

Ade13 is an adenylosuccinate lyase that catalyzes two steps in the purine nucleotide biosynthesis pathway (Dorfman 1969). Purine nucleotides such as guanosine triphosphate (GTP) and adenosine triphosphate (ATP) function as energy storage units, constitute nucleic acids and play an important role in signaling cascades. The diverse roles of purine nucleotides cement *ADE13* as an essential gene for its role in the *de novo* production of these molecules. Since its isolation in the 1970s, studies have sought to define its interactions and roles in *S. cerevisiae.* The essential role of Ade13 in the purine biosynthesis pathway is to convert succinyl amino imidazole carboxamide ribonucleotide monophosphate (SZMP) to amino imidazole carboxamide ribonucleotide monophosphate (ZMP). ZMP is the precursor to inosine monophosphate (IMP), which is then used to synthesize succinyl adenosine monophosphate (SAMP). Finally, Ade13 also catalyzes the step from SAMP to adenosine monophosphate (AMP) (Daignan-Fornier and Pinson 2019). Ade13 expression is inhibited by adenine and facilitated by Pho2 (Phosphate metabolism) and Bas1 (Basal). Pho2 and Bas1 are both transcription factors that are associated with the regulation of phosphate metabolism and purine/histidine biosynthesis pathways, respectively (Denis et al. 1998; Lenburg and O'Shea 1996). Because of its essential nature and importance at the cellular level, the purine biosynthesis pathway remains relatively conserved across eukaryotes. So much so that the Ade13 amino acid sequence is 79% similar to the human ortholog Adsl (Daignan-Fornier and Pinson 2019). Mutation of the ortholog Adsl in humans leads to adenylosuccinate lyase deficiency (ADSL deficiency) and is due to a loss of function in Adsl and is displayed in an autosomal recessive fashion (Jaeken and Berghe 1984).

Gid10

Gid10 is a subunit of the glucose-induced degradation (GID) ubiquitin ligase of the Pro/N-degron pathway that recognizes N-terminal degradation signals (Melynkov et al. 2019). In growing conditions with low levels of glucose, yeast cells are forced to perform gluconeogenesis to produce glucose. Expression of multiple gluconeogenesis-related enzymes such as the phosphoenolpyruvate carboxykinase (Pck1), malate dehydrogenase (Mdh2), fructose-1,6-biphosphatase (Fbp1), and isocitrate lyase (Icl1) must be synthesized to enable gluconeogenesis (Varshavsky 2019). However, once glucose becomes available again, these enzymes are subjected to controlled degradation. The degradation of these enzymes is known to be mediated by the GID ubiquitin ligase. GID ubiquitin ligase consists of Gid1, Gid2, Gid4, Gid5, Gid7, Gid8, and Gid9 subunits. Gid10 is similar to Gid4 in function and has an overlap in substrate specificity. Both Gid10 and Gid4 function to recognize substrates containing N-terminal proline residues for degradation via GID ubiquitin ligase and the proteasome (Chen et al. 2017). The difference between the two lies in Gid10 expression only under starvation or osmotic stress and acts as an alternative recognition factor in the Pro/N-degron pathway (Melynkov et al. 2019).

Fsh3

Fsh3 was discovered by Baxter et al. (2004) as a member of the eukaryotic serine hydrolase family, which also defines the notation of the protein as a family of serine hydrolase (Fsh). As a serine hydrolase, Fsh3 structurally possesses a serine active site, and the specific function of the protein can be categorized into multiple subclasses: proteases, lipases, esterases, transacylases, and lyases (Baxter et al. 2004). The delineation of each of these subclasses can typically be determined through amino acid sequence analysis and subsequent comparison to structural data in the Protein Data Bank (PDB). Unlike Fsh1 and Fsh2, which contain lipase motifs, Fsh3 does not and was documented as a putative lipase (Baxter et al. 2004), and additional

sequence analysis uncovered a peroxisomal targeting sequence (PTS1) within Fsh3 (Notzel et al. 2016). The peroxisomal targeting sequence suggests the potential localization of Fsh3 within *S. cerevisiae.*

To investigate the localization of Ade13, Gdi10, and Fsh3 in *Saccharomyces cerevisiae*, we took an experimental approach similar to the work by Huh et al. (2003) First, we used phylogenetic analyses that compare amino acid sequences of the yeast proteins to other species with known localization data to predict the localization of each protein in *S. cerevisiae*. Then, we modified the open reading frame of each gene at the 3' end by adding a C-terminal green fluorescent protein (GFP) tag. The live cells expressing the GFP fusion proteins were subjected to direct fluorescence microscopy, and the localization of fusion proteins was examined.

Methods

Phylogenetic Analysis

Phylogenetic relationships were inferred based on the amino acid sequences of orthologous proteins sampled from four other model organisms as well as *Saccharomyces cerevisiae*. Using the *Saccharomyces* Genome Database (SGD), orthologs for each protein were identified in *Caenorhabditis elegans, Drosophila melanogaster*, *Rattus norvegicus*, *Mus musculus*, and *Homo sapiens* and collected via the NCBI HomoloGene database (https://www.ncbi.nlm.nih.gov/homologene). Amino acid sequences were then aligned in AliView using Multiple Sequence Comparisons by Log-Expectation (MUSCLE). (Larsson 2014; RC Edgar 2004). Next, localization data downloaded from the Alliance of Genome Resources database (https://www.alliance genome.org/) was paired with each of the five species. After alignment, we inferred phylogenetic relationships using maximum likelihood estimation as implemented in the

online EMBL-EBI Simple Phylogeny Software (Madeira et al. 2022). Default tree format and maximum likelihood estimation methods were selected as the parameters to infer phylogenetic relationships. We conducted non-parametric bootstrapping to assess the support of nodes with 10,000 bootstrap replicates. Inferred trees and localization data were then analyzed in R using the PhyTools package (Revell 2012).

Bacterial/Yeast Strains and Media

The *Escherichia coli* and *Saccharomyces cerevisiae* strains used in this study are listed in Table 1. All *E. coli* strains were grown on LB medium containing 50µg/ml ampicillin (BD laboratories Inc., Franklin Lakes, NJ). *S. cerevisiae* strains were grown using four different media. Yeast extract Peptone Dextrose (YPD) media was made using the premixed powder (Dipco) which contains 1% Bacto-yeast extract, 2% Bacto-peptone, and 2% glucose. Yeast Extract Peptone (YEP) media was made using 1% Bacto-yeast extract, 1% Bacto-peptone, and 0.5% sodium chloride. Synthetic complete (SC) media was made using 0.67% Bacto-yeast nitrogen without amino acids (Difco Laboratories, Inc.), 2% glucose, 0.2% Histidine drop-out powder (BD Laboratories Inc.), and 0.002% (20mg/L) L-Histidine HCl (BD Laboratories Inc.). Synthetic Complete-Histidine drop-out (SC-His) media was made using 0.67% Bacto-yeast nitrogen without amino acids (Difco), 2% glucose, and 0.2% Histidine drop-out powder. In addition to broth, all media was made into agar via the addition of 2% Bacto-agar. All media was stored at 4ºC excluding YPD broth, which was stored at 20ºC.

C- terminal Tag Strain Construction

The template plasmid DNA extraction for tagging was performed by following the standard protocol for the Monarch Plasmid Miniprep kit (New England Biolabs Inc., Ipswich, MA). PCR cassette amplification was performed using One*Taq* quick Load 2x Master Mix with Standard Buffer (New England BioLabs Inc., Ipswich, MA). The primer design utilized the Primers-4-Yeast website (Yofe and Schuldiner 2014) where gene-specific 3' tags were amplified via PCR. The final 50µL PCR mixtures contained; 10ng EFB174 pFA6 mini-prepped DNA template, 25µL One*Taq* quick Load 2x Master Mix with Standard Buffer, 1µL (10µM) forward primer, 1µL (10µM) reverse primer and 22µL ddH_2O. Gene-specific forward and reverse primers for each gene are listed in Table 1. The PCR cycle setup was implemented using an initial denaturation for 30 seconds (s) at 94ºC followed by 30 cycles of denaturation for 30s at 94ºC, annealing for 60s at 45ºC, and extension for 120s at 68ºC. The final extension period was 300s at 68ºC and was held at 4ºC. Per PCR, a negative control that withheld the pFA6 plasmid DNA template was included for each PCR reaction. PCR products were resolved on 1.5% TBE gel. Verified PCR products were purified using Monarch PCR DNA Cleanup Kit (New England BioLabs Inc., Ipswich, MA), following the manufacturer-provided protocol. Purified DNA concentration was determined using Qubit 1x dsDNA HS Assay Kit (Thermo Fischer Scientific Inc., Waltham, MA).

The 3' gene-specific *GFP-HIS3* tags were transformed into *S. cerevisiae* wild-type strain (BY4741) by adding 1.5 µg of the amplified cassette DNA to 5 OD units of cells in early log phase. Cells were transformed via a high-efficiency yeast transformation protocol that used lithium-acetate (LiAc), polyethylene glycol (PEG), and single-stranded DNA (Cold Spring Harbor Laboratory Course Manual, 2015). Transformed cells were grown on SC-His plates at 30ºC for 4-5 days and individual colonies were streaked onto SC-His plates.

Individual colonies were examined for proper integration via colony PCR. Primers for C' tag check and validation were designed using Primers-4-Yeast (Yofe and Schuldiner 2014). Genomic DNA was isolated from each colony as a template, and the final 25µL PCR mixtures contained; 1.0 µg genomic DNA template, 12.5µL One*Taq* quick Load 2x Master Mix with Standard Buffer, 0.5µL (10µM) forward CHK primer, 0.5µL (10µM) reverse CHK primer and 10.5µL ddH_2O. Untransformed yeast genomic DNA was used as a negative control for confirmation PCR. PCR products were resolved on 1.5% TBE gel.

Growth Analysis

The growth of individual transformants was monitored for 48 hours at 30ºC. Cells were grown in YPD, and an aliquot was taken every two hours for the first 12 hours and, after that, every four hours during the final 36 hours for optical density measurement at 600nm of wavelength using Genesys 10S UV-Vis Spectrophotometer (Thermo Fischer Scientific Inc., Waltham, MA). OD600 measurements were plotted using R Studio and a trend line was fit using locally estimated scatterplot smoothing. The spotting analysis was performed using *S. cerevisiae* wild-type strains and individual colonies of GFP-tagged cells, LBYA4a, LBYA8a, LBYA3b, LBYA4b, LBYF6, and LBYG1 strains. Two OD units of cells from each strain in 10-fold serial dilutions were spotted on YPD plates and incubated at 30ºC for 2 days before image capture.

Fluorescence Microscopy

Yeast transformants with C-terminal GFP tag were grown at 30°C in SC-His media and were harvested in the early log phase and resuspended in cold 1x PBS for fluorescence imaging. For mitochondrial imaging, 2mL of cell cultures were inoculated with 0.4 µL Mitotracker Red CMXRos (Cell Signaling Technology, Beverly, MA). 300 µL of cell culture containing 1.6x10^8

cells were resuspended in 200 µL cold 1x PBS. Before imaging, 5 µL of cell/1x PBS solution was mixed with 2 µL EverBrite Mounting Medium with DAPI (Biotium Inc. Fremont, CA). Cells were observed in Zeiss A1 Axioscope with an X-cite xenon light source, and images were taken using an AxioCamMR3 with a 63x oil 1.3 NA Plan-Neoflaur objective lens. In addition to the fluorescence images taken, DIC images were collected for each strain. Images were taken and downloaded from Axiovision Software (Carl Zeiss Microscopy). Fluorescent cell counts were made by collecting images containing 100 cells and determining the percentage of cells showing specific fluorescence signals. GFP-tagged trains were imaged using GFP, DAPI, and Mitotracker Red excitation and emission filters.

Fluorescence Analysis

ImageJ (Schneider et al. 2012) was used to perform fluorescence analysis of images, and captured images were visualized and cropped to overlap. Colocalization images were created and analyzed using Just Another Colocalization Plugin (JACoP) (Bolte and Cordelieres 2006) and Colocalization Finder (Laummonerie et al. 2004). JACoP was used to determine Pearson's Coefficient, Manders' Coefficient, cytofluorogram, and pixel fluorogram for each fluorescence image.

Results

Phylogenetic Comparative Analysis

We performed a preliminary analysis of protein localization based on evaluating the amino acid sequences of orthologous proteins in seven model organisms: *Saccharomyces pombe, Caenorhabditis elegans, Drosophila melanogaster, Rattus norvegicus, Mus musculus, Danio rerio,* and *Homo sapiens.* Amino acid sequence alignment showed a sequence similarity of 71.7%

between *S. cerevisiae* (Fsh3) and its human ortholog (Ovca2), 47.4% between Gid10 and Gid4, and 79.2% between Ade13 and Adsl (Figure 1) Fsh3 alignment length was 4841, Gid10 alignment length was 345, and Ade13 alignment length was 490.

To assess the evolutionary history of Fsh3, Gid10, and Ade13, aligned amino acid sequences were compared via phylogenetic analysis (Figure 2). From the analysis, inferred evolutionary relationships were used to compare localization data. Fsh3, Gid10, and Ade13 were predicted to localize to the cytoplasm and/or nucleus, and, in the case of Ade13, the analysis also showed potential mitochondrial localization.

C-terminal

Tagging and Growth Analysis

To examine the localization of each protein via fluorescence microscopy, we modified the protein gene by integrating a gene cassette containing the Green Fluorescence Protein (GFP) gene and a selection marker at the 3' end, which is a well-established method in *S. cerevisiae* (Longtine, 1998). The modification results in a GFP fusion protein (Figure 3) and can be visualized via live cell imaging. However, modification of endogenous genes can pose potential disruption of protein conformation and function, especially when the genes are essential, and can cause modified cells to be sick or unviable. Therefore, it was important to ensure that C-terminally GFP-tagged yeast strains grow comparably to wild-type cells. To monitor the growth rate, cells were grown in YPD at 30ºC continuously, and the optical density of the culture was measured at 600 nm throughout the logarithmic phase of growth. Both Gid10-GFP and Fsh3-GFP strains grew comparably to the wild-type strain while the Ade13-GFP strain appeared to display growth delay during the early phase of logarithmic growth (Figure 4). To determine whether Ade13 is disrupted by GFP tagging

or if the individual colony had a variable growth defect for unknown reasons, the growth of multiple Ade13-GFP colonies was monitored (Figure 5). The delayed growth appeared to be specific to the colony chosen in the earlier growth measurement experiment and additional colonies grew comparably to the wild-type strain. Additionally, a spotting assay was performed to visualize the growth of multiple Ade13-GFP, Gid10-GFP, and Fsh3-GFP strains. Spotting assay allows visualization of individual colony size besides overall growth, which may be masked from growing cells in liquid culture and measuring the optical density of aliquots of the culture. The spotting assay results were consistent with the growth curve experiments and confirmed that LBYA8a was the only Ade13-GFP colony with compromised growth (Figure 6).

Fluorescence Images and Analysis

Fsh3

To examine the cellular localization of Fsh3, a DAPI fluorescent stain was used to assess the cytoplasmic prediction made in the preliminary phylogenetic study. Fsh3-GFP displayed a dispersed cytoplasmic GFP fluorescence but also were observed in distinct puncta throughout the cytoplasm (Figure 7). This unique localization pattern was observed in 73.54 ± 1.78% of cells (n=300). Analysis of the merged image of GFP and DAPI fluorescence showed low overlap in fluorescence and supported that Fsh3-GFP was not localized to the nucleus. Following the visual observation of merged images, a quantitative approach using ImageJ was taken to determine fluorescent overlaps and colocalization. Cytofluorogram modeling determined there was a Pearson's correlation coefficient of 0.356 between DAPI and GFP fluorescence. Pearson's correlation coefficients range from 0-1 and are the slope of the cytofluorogram. The value of 0.356 supported the qualitative observation of low overlap between DAPI and Fsh3-GFP. To further determine if there was any overlap between fluorescence signals, analysis of the colocalization

images using Manders' Coefficients identified values of 0.479 for DAPI overlapping GFP and 0.212 for GFP overlapping DAPI. This showed that while there was a slight overlap, the majority of Fsh3-GFP fluorescence signals did not overlap with DAPI.

Gid10

To test the initial prediction of cytoplasmic or nucleic localization, Gid10-GFP fluorescence was compared to a DAPI nuclear stain. When grown in YPD at 30ºC Gid10-GFP localized diffusely throughout the cytoplasm (Figure 8). This fluorescent pattern could be seen in 61.67 ± 2.31% of cells (n=300). Further quantitative analysis of this pattern included cytofluorogram visualization of the merged image and showed a Pearson's correlation coefficient of 0.272 between DAPI and GFP fluorescence, and Manders' Coefficients of 0.115 for DAPI overlapping GFP and 0.057 for GFP overlapping DAPI. These findings supported that there was little overlap between the nucleus and Gid10-GFP.

Due to the proposed role that Gid10 plays within the GID complex regarding gluconeogenesis, we hypothesized that a change in Gid10 function based on glucose availability may also alter the cytoplasmic localization of the protein. To test the hypothesis, Gid10-GFP cells were grown in YEP media, which has no glucose, for comparison of localization. Generally, when the Gid10-GFP strain is grown in YPD, the diffusive GFP fluorescence was primarily cytoplasmic. However, when the same strain was grown in YEP, Gid10-GFP was concentrated in small puncta throughout the cytoplasm. The cytoplasmic puncta were found in 35.13 ± 6.43% of cells (n=300) (Figure 9). Cytofluorogram and pixelfluorogram visualization of the colocalization between DAPI and GFP fluorescence showed a Pearson's correlation coefficient of 0.360 and Manders' Coefficients of 0.008 for DAPI overlapping GFP and 0.011 for GFP overlapping DAPI.

Comparative fluorescence analysis indicates that the puncta observed in Gid10-GFP cells under glucose depletion is not the nucleus of the cell.

Ade13

As in the case of Gid10 and Fsh3, Ade13 was predicted to localize to the nucleus and cytoplasm. Preliminary fluorescence microscopy of Ade13 cells displayed a diffusive cytoplasmic localization while no nuclear localization was evident. Interestingly, an Ade13 ortholog in *D. melanogaster* has been documented to localize to the mitochondria, and we decided to examine the localization more carefully, especially concerning mitochondria using the mitochondrial stain, Mitotracker Red. Indeed, direct immunofluorescent imaging of live Ade13-GFP cells supported the cellular localization of Ade13 to the mitochondria (Figure 10). Contrary to our expectation, fluorescence signals showed an uneven distribution throughout the cell, and Mitotracker red staining of the mitochondria displayed a similar pattern. The merged image indicated strong colocalization between the fluorescent micrographs taken under FITC and TRITC filters, and the GFP fluorescence pattern can be seen in 85.96 ± 1.89% of cells (n=300). To corroborate these findings, cytofluorogram modeling showed a 0.756 Pearson's correlation coefficient and Manders' Coefficients of 0.854 for Mitotracker Red overlapping GFP and 0.792 for GFP overlapping Mitotracker Red. These analyses indicate high levels of overlap and support the finding of Ade13-GFP localization to the mitochondria.

Discussion

We aimed to fill the remaining knowledge gaps concerning the cellular localizations of Fsh3, Gid10, and Ade13, and we sought to predict the localization of each protein selected via phylogenetic analysis of the amino acid sequences. Through our analysis, we predicted that Fsh3,

Gid10, and Ade13 would localize to either the nucleus or the cytoplasm. Uniquely, Ade13 could also localize to the mitochondria. The preliminary study also showed the conserved nature of our selected proteins to each ortholog in humans. With the predicted localization data acquired from the preliminary study, the project's main goal to identify the cellular localization of Ade13, Fsh3, and Gid10 could begin.

Past studies have shown the efficacy of C-terminal GFP tagging in the analysis of protein localization in *S. cerevisiae* (Huh et al. 2003). Our study took a similar approach in investigating and validating our hypothesized localization predictions of Fsh3, Gid10, and Ade13. Prior to microscopy, we confirmed that GFP tagging did not have a negative effect on the viability of cells and presumed that the functions of tagged proteins were not negatively affected.

Based on our comparative phylogenic prediction, Fsh3, a serine hydrolase, was predicted to localize to the cytoplasm or nucleus. In all compared model organisms, reported localization suggested that Fsh3 orthologs localize to the nucleus/cytoplasm. We found that Fsh3 localized to distinct cytoplasmic puncta, indicating that Fsh3-GFP does not localize to the nucleus as predicted (Figure 7). Before we were able to identify the specific nature of these puncta, a recent study by Yifrach et al. (2022) reported Fsh3 localizes to the peroxisome and functions as a lipase. The fluorescence results in this study were consistent with our findings and their methods can be used in the future to corroborate these results. Cytofluorogram modeling of overlapping fluorescence images using Pearson's Coefficient as a correlation coefficient displays a low value of 0.356, meaning that Fsh3-GFP and DAPI nuclear stains do not colocalize.

The role of Fsh3 in *S. cerevisiae* was initially examined by Baxter et al. (2014), and further studies have identified orthologs in other model organisms. Of the organisms selected for comparative analysis, a human gene was determined to be similar to the *S. cerevisiae* gene. The

human gene, Ovarian tumor suppressor candidate 2 (*OVCA2*), aligned with *FSH3*, and showed a high BLAST E-value of $5x10^{-10}$, indicating a relatively high sequence similarity between the two genes. The locus of OVCA2 is known to be in chromosome region 17p13.3. Interestingly, this particular region has been documented to be deleted in 80% of instances of ovarian cancer (Phillips et al. 1993). Ovca2 is still listed as a candidate for tumor suppression, but the mechanistic detail of the protein function and its localization are still elusive. The peroxisomal localization of Fsh3 may serve as preliminary data for future studies on Ovca2 and its localization within the human cell. A better understanding of its role as a peroxisomal lipase may give rise to new questions. How do Fsh3 and Ovca2 compare in localization? The Alliance of Genome Resources reports Ovca2 to localize to the cytoplasm, and therefore further research is necessary to elucidate a more definitive observation.

Based on amino sequence analysis of orthologs, Gid10 was predicted to localize to the cytoplasm or nucleus. As in the case of Fsh3, our comparative analysis displayed the same prediction in all compared organisms. The glucose-dependent role of Gid10 produced a particular line of questioning for identifying cellular localization. We found that under glucose-rich conditions Gid10-GFP was diffused throughout the cytoplasm, but when glucose is depleted, Gid10-GFP becomes sequestered or limited to distinct cytoplasmic puncta. Through our fluorescence analysis, we confirmed that these puncta indeed did not overlap with the nucleus. The alteration of localization under different nutrient conditions can be explained by the role Gid10 plays in the glucose-induced degradation (GID) pathway.

Gid10 functions as a ubiquitin ligase and polyubiquitinates gluconeogenic proteins for eventual degradation via the proteasome (Regelmann et al. 2003). Under high glucose conditions, gluconeogenic enzymes are not necessary for metabolism, and therefore the GID complex would

actively mark these related proteins for proteolysis, explaining the cytoplasmic localization of Gid10-GFP. Under low-glucose conditions, however, gluconeogenic proteins are required for cell viability. The sequestration of Gid10 would prevent the polyubiquitination and subsequent proteolysis of gluconeogenic enzymes via the proteasome. Interestingly, the recent study by Yifrach et al. (2022) reported GFP-Gid7 to localize to the peroxisome under gluconeogenic conditions. Gid7 is also a component of the GID complex, and by association, suggests the localization of Gid10 to be peroxisomal. Therefore, it might be fruitful for future colocalization studies to examine Pex3-GFP (Figure 3) and Gid10-GFP under different glucose concentrations.

Gid4, a human ortholog of Gid10, is predicted to have ubiquitin ligase activity. In humans, *GID4* is located on chromosome 17, and genetic mutations within the regions containing 17p11.2 are associated with multiple genetic disorders, one of them being Smith-Magenis Syndrome (SMS). SMS is also associated with the deletion of *RAI1*, and individuals affected are typically diagnosed with multiple congenital anomalies such as skeletal abnormalities, speech and developmental delay, and hypotonia (Elsea and Girirajan 2008). While this particular developmental disorder is largely associated with the deletion of the retinoic acid-induced (*RAI1*) gene, not all the features associated with SMS have been linked to the deletion of *RAI1*. Duplications of the 17p11.2 region lead to Potocki-Lupski syndrome (PTLS) and can be associated with the duplication of multiple at-fault genes *PMP22, FCLN, RAI1,* and other unknown genes (Potocki et al. 2007). PTLS-affected humans are described by delayed development, intellectual disabilities, and behavioral abnormalities. *RAI1* is observed as the most common denominator in many of the diseases, and its potential role as a source of pathogenicity upon deletion or duplication in tandem with additional genes should be explored, including the proximal *GID4* gene. Further confirmation of Gid10's cellular localization would be useful in understanding Gid4 and its role

in diseases associated with mutations in the 17p11.2 region. Specifically, interactions and colocalization with the peroxisome should be investigated, and until confirmation of Gid10 localization can be completed, further comparisons between Gid10 and Gid4 cannot be made.

Our predictions indicated that Ade13 orthologs localize to the cytoplasm or nucleus in most organisms, but mitochondrial in *D. melanogaster*. The initial assessment of Ade13-GFP cells raised concern about the effects of the C-terminal tagging on fusion protein function and cell viability. Of the 16 initial transformants, four had confirmed integration through colony PCR; LBYA4a, LBYA8a, LBYA3b, and LBYA4b. Overnight cultures of LBYA8a for microscopy indicated that the strain was not aligning with typical growth assumptions, and had an average doubling time of 3.76 hours, while the typical doubling time of the wt strain was 1.5 hours. This finding established a question of whether the C-terminal tag was inhibiting the natural function of Ade13, which is essential. Subsequent growth rate analysis and spotting assays determined that this atypical growth behavior was limited to LBYA8a, so LBYA4b was selected for fluorescence imaging. The mitochondrial stain (Mitotracker Red) was used to perform colocalization analysis on Ade13-GFP, and we found that Ade13 localizes to the mitochondria in *S. cerevisiae*. Our colocalization analysis and cytofluorogram visualization support this claim through reports of a high Pearson's Coefficient of 0.756.

As an adenylosuccinate lyase, Ade13 plays a pivotal role in purine nucleotide biosynthesis. One major role and function of purine nucleotides is their role as energy storage in the form of triphosphate molecules such as guanosine triphosphate (GTP) and adenosine triphosphate (ATP). Its role in the purine biosynthesis pathway is conserved in humans and is referred to as Adsl. Mutation of the ADSL gene leads to adenylosuccinate lyase deficiency (ADSL deficiency) and is associated with psychomotor delay or autistic features (Camici et al. 2009). The disease manifests

in many ways and includes the symptoms of seizures, acute or chronic encephalopathy, behavioral abnormalities, and dysmorphic features (Jurecka et al. 2015). ADSL deficiency is categorized in three ways type I, type II, and fatal form. Type I is known as a severe form and presents itself in the first few months of life. Type II is mild or moderate and occurs in the first few years of life. Lastly, the fatal form is the most severe leading to respiratory failure and seizures that eventually lead to death. ADSL deficiency has been reported an estimated number over 60 times since its discovery in 1984 (Jurecka et al. 2015), and regardless of its rarity, research should be made to better understand the disease regarding the human purine biosynthesis pathways. The identification of Ade13-GFP localization to the mitochondria can lead to new questions regarding the recorded cytoplasmic localization of Adsl. Why does the localization of each protein change between *S. cerevisiae* and *H. sapiens*? Should Adsl localization be reassessed? Further studies should be performed to determine how Ade13 and Adsl localization can be compared.

Future Directions

In this study, we identified Ade13-GFP localization to the mitochondria and assessed the interference of fluorescent tagging with the natural function of the protein. We performed growth analyses to determine the viability of modified cells as a measure of assumed proper protein expression and function in the cell, but Western-Blot analysis would confirm the existence of fully expressed fusion proteins, which should be conducted for all three proteins in this study. As for Gid10 and Fsh3, an investigation to reveal the identity of puncta, which we hypothesized to be the peroxisome should be performed. The logical approach would be to tag a peroxisomal protein, such as Pex3, with a different fluorescence tag to conduct a colocalization analysis (Figure 3)

In conclusion, we identified the localization of Ade13 to the mitochondria. The identification of cytoplasmic puncta in Gid10-GFP and Fsh3-GFP provides a new avenue for

exploration, and, in combination with related studies (Yifrach et. At 2022), more of the yeast proteome can be localized. More broadly, understanding localization will allow us to gain a new understanding of protein function and interactions that are tied to protein localization in *Saccharomyces cerevisiae.* With this, we may gain novel insight into orthologous proteins related to human disease in conserved basic processes.

Appendix 1 Tables

Table 1: List of Bacteria and Yeast Strains used in the study.

Strain	**Genotype**	Remarks
EFB174	pFA6 (Longtine et al. 1998) containing GFP-His3	*E. coli*
EFB178	pFA6 containing dtomato-KanMX	*E. coli*
BY4741	*MATa his3Δ1 leu2Δ0 met15Δ0 ura3Δ0*	*S. cerevisiae*
LBYA4a	*MATa his3Δ1 leu2Δ0 met15Δ0 ura3Δ0 ADE13-GFP::HIS3*	*S. cerevisiae*
LBYA8a	*MATa his3Δ1 leu2Δ0 met15Δ0 ura3Δ0 ADE13-GFP::HIS3*	*S. cerevisiae*
LBYA3b	*MATa his3Δ1 leu2Δ0 met15Δ0 ura3Δ0 ADE13-GFP::HIS3*	*S. cerevisiae*
LBYA4b	*MATa his3Δ1 leu2Δ0 met15Δ0 ura3Δ0 ADE13-GFP::HIS3*	*S. cerevisiae*
LBYF3	*MATa his3Δ1 leu2Δ0 met15Δ0 ura3Δ0 FSH3-GFP::HIS3*	*S. cerevisiae*
LBYF6	*MATa his3Δ1 leu2Δ0 met15Δ0 ura3Δ0 FSH3-GFP::HIS3*	*S. cerevisiae*
LBYG1	*MATa his3Δ1 leu2Δ0 met15Δ0 ura3Δ0 GID10-GFP::HIS3*	*S. cerevisiae*
LBYG2	*MATa his3Δ1 leu2Δ0 met15Δ0 ura3Δ0 GID10-GFP::HIS3*	*S. cerevisiae*

Name	Primer	Sequence (5'-3')
ADE13 C' GFP-HIS3 tag	Forward	CCAAAAGTACCTAAACGATG AACAAGTCAAGTTAAATGTT CGGATCCCCGGGTTAATTAA
	Reverse	AGGGTAATAAACATATTATT TGTACATGTAAAGGCTTCTA GAATTCGAGCTCGTTTAAAC
GID10 C' GFP-HIS3 tag	Forward	CGACGCATTGAACACCTACTC AAGTGGATTTGAAATTGCCC GGATCCCCGGGTTAATTAA
	Reverse	AGTAAACAAACATACATTGG TAATTCTATAAGGGTCTTTA GAATTCGAGCTCGTTTAAAC
FSH3 C' GFP-HIS3 tag	Forward	AGATGATTTGTTAGATATGA TCGATTCCTTGGGTAAATTG CGGATCCCCGGGTTAATTAA
	Reverse	AAATTGTATGTAGCTCATAT AAATATCAATTATCGAATTA GAATTCGAGCTCGTTTAAAC
PEX3 C' dtomato-KanMX tag	Forward	CAGCAACTTTGGCGTCTCCAGCTCGTTTTC CTTCAAGCCTCGGATCCCCGGGTTAATTA A
	Reverse	ATATATTCTGGTGTGAGTGTCAGTACTTAT TCAGAGATTAGAATTCGAGCTCGTTTAAA C
ADE13 C' tag CHK	Forward	TCAATGGTTCGAAAGAACTC
GID10 C' tag CHK	Froward	GTTTGGTCATTTTGGTTCTG
FSH3 C' tag CHK	Forward	CCATTTGATGGTGTCATTG
PEX3 C' tag CHK	Forward	CACGAATTCCCAAATATTCC
pFA6 C' tag CHK Compliment	Reverse	TTAATTAACCCGGGGATCCG

Table 2: List of Primers for PCR

Appendix 2 Figures

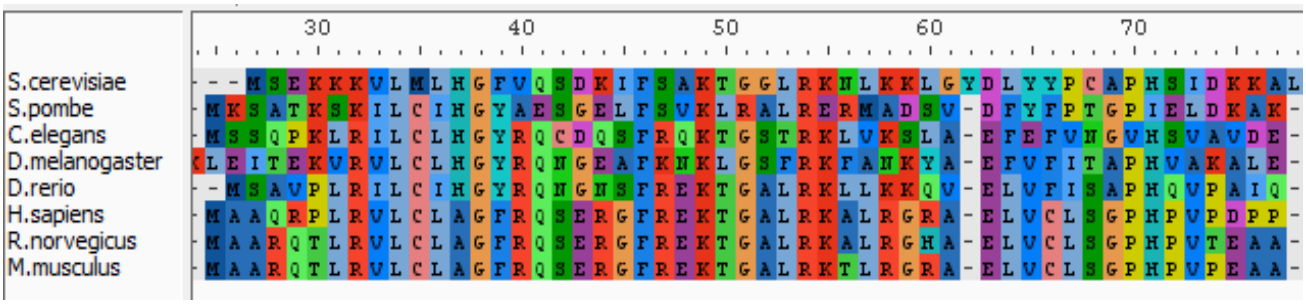

Figure 1. Sequence (Fsh3) alignment via Aliview shows conserved patches of amino acids. Sequence Data collected from NCBI (Homologene 2022). Amino acid coloring: Hydrophobic (Blue), Positive charge (Red), Negative charge (Magenta), Polar (Green), Cysteines (Pink), Glycines (Orange), Prolines (Yellow), Aromatic (Cyan).

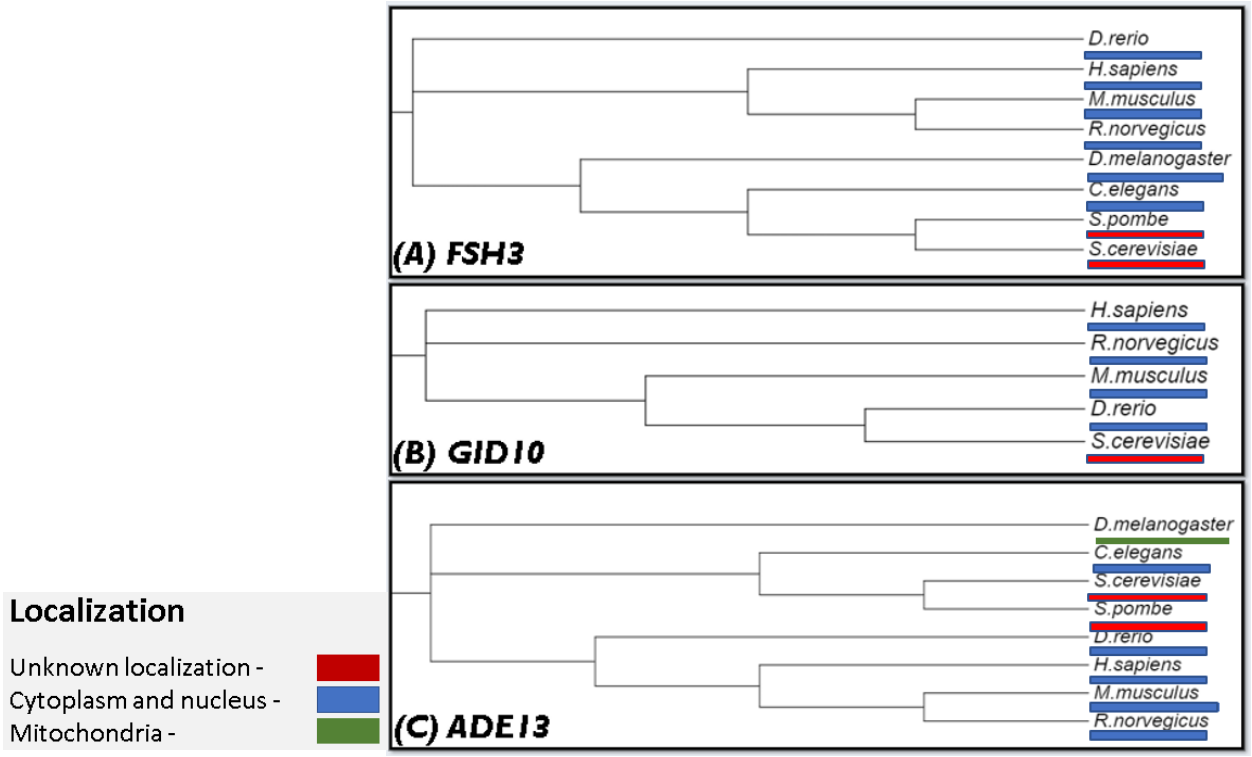

Figure 2. Fsh3 and Gid10 are predicted to localize to the cytoplasm and nucleus, while Ade13 is predicted to localize to the mitochondria. Inferred trees and localization data were used to predict the localization of Fsh3, Gid10, and Ade13. (A) Fsh3 amino acid sequence phylogeny. (B) Gid10 amino acid sequence phylogeny. (C) Ade13 amino acid sequence phylogeny.

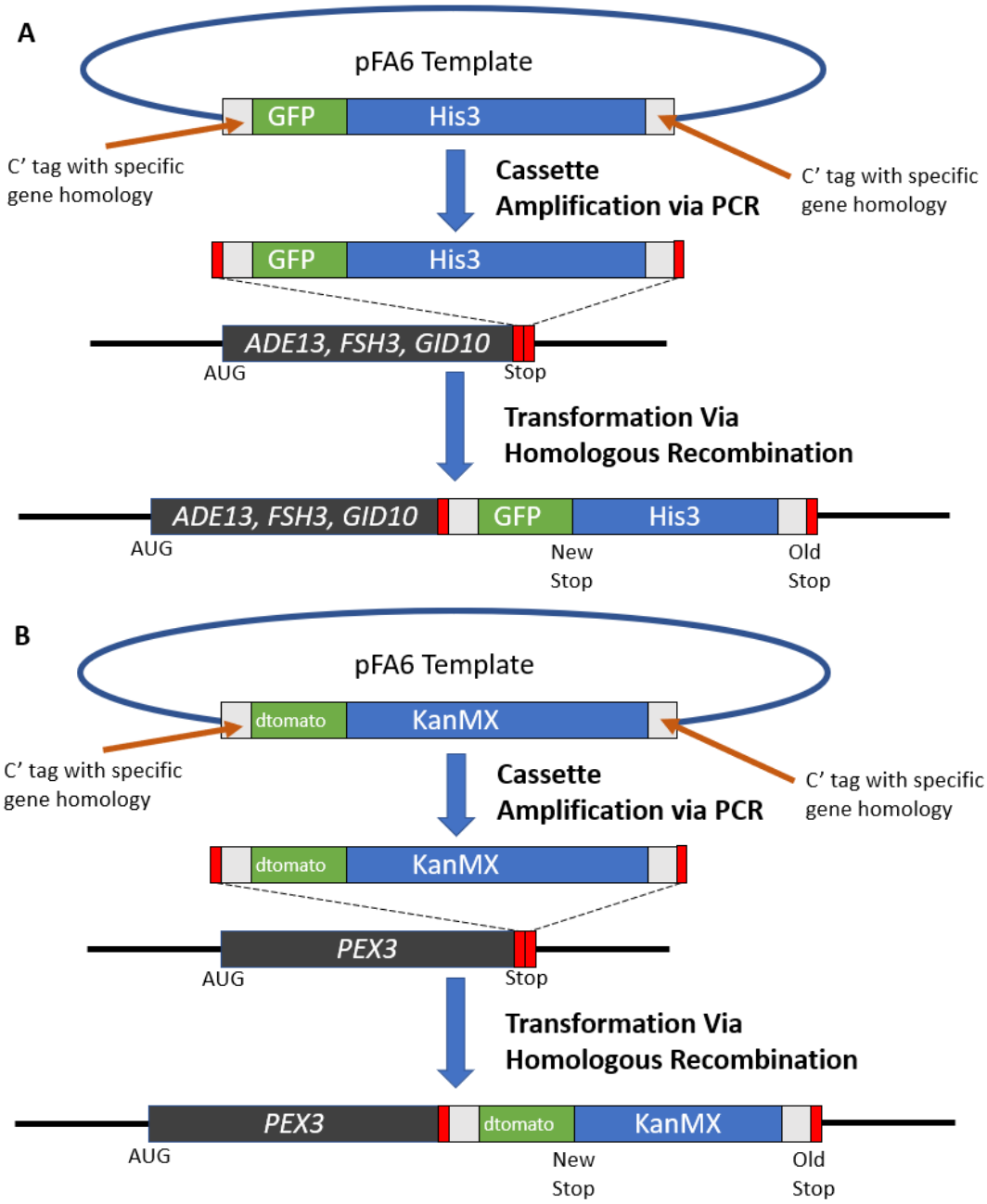

Figure 3. C-terminal GFP tag construction via cassette PCR and genomic integration. Yeast strains were constructed using the Longtine method which is designed to integrate the cassette at the 3' end of the endogenous genes of interest. The proper integration of the cassette was confirmed via colony PCR (Longtine et al. 1998). (A) C-terminal GFP tag creation for *ADE13, FSH3, and GID10.* (B) C-terminal tomato tag creation for *PEX3.*

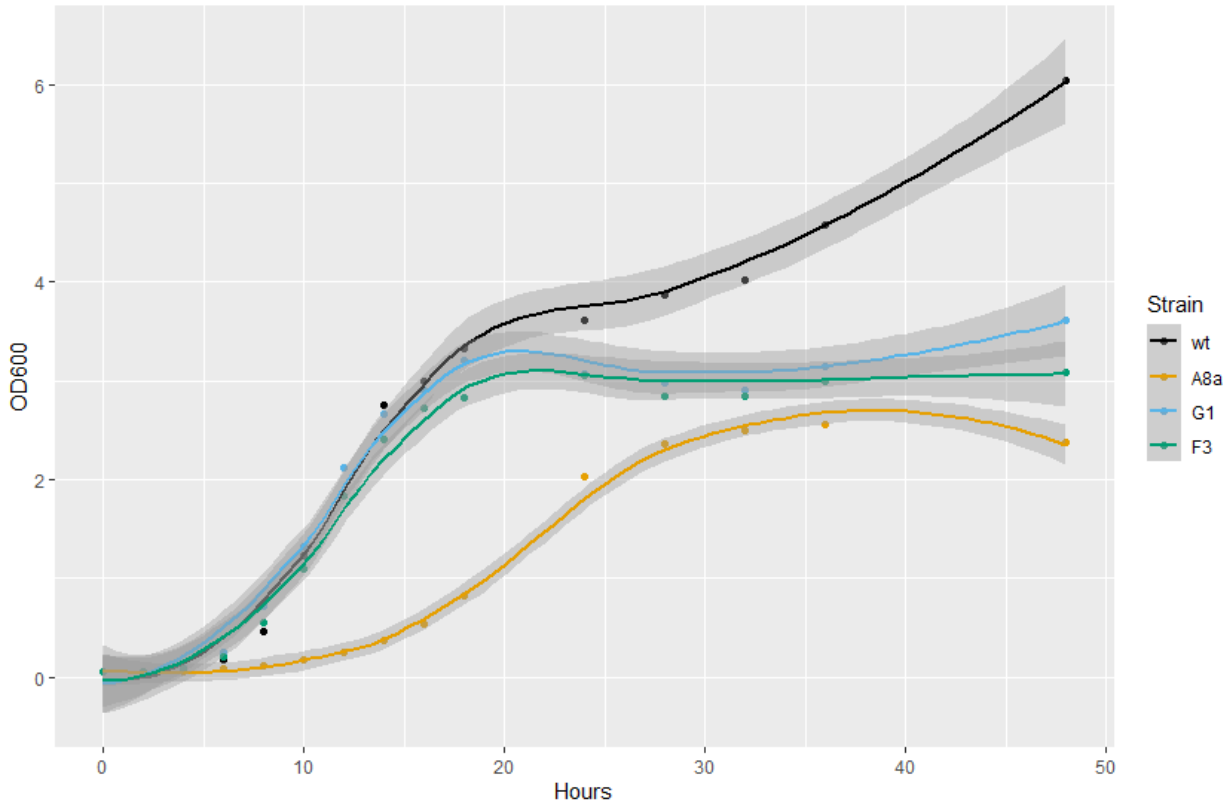

Figure 4. Growth rate measurement of C-terminally GFP tagged strains over 48 hours. A colony from each of the three C-terminally tagged strains was grown in YPD continuously at 30ºC with aeration and an aliquot was taken every 2 hours for optical density (OD) measurement at 600nm wavelength of light. The OD reading was plotted against time and the growth rate was compared to wild type (B4741) strain.

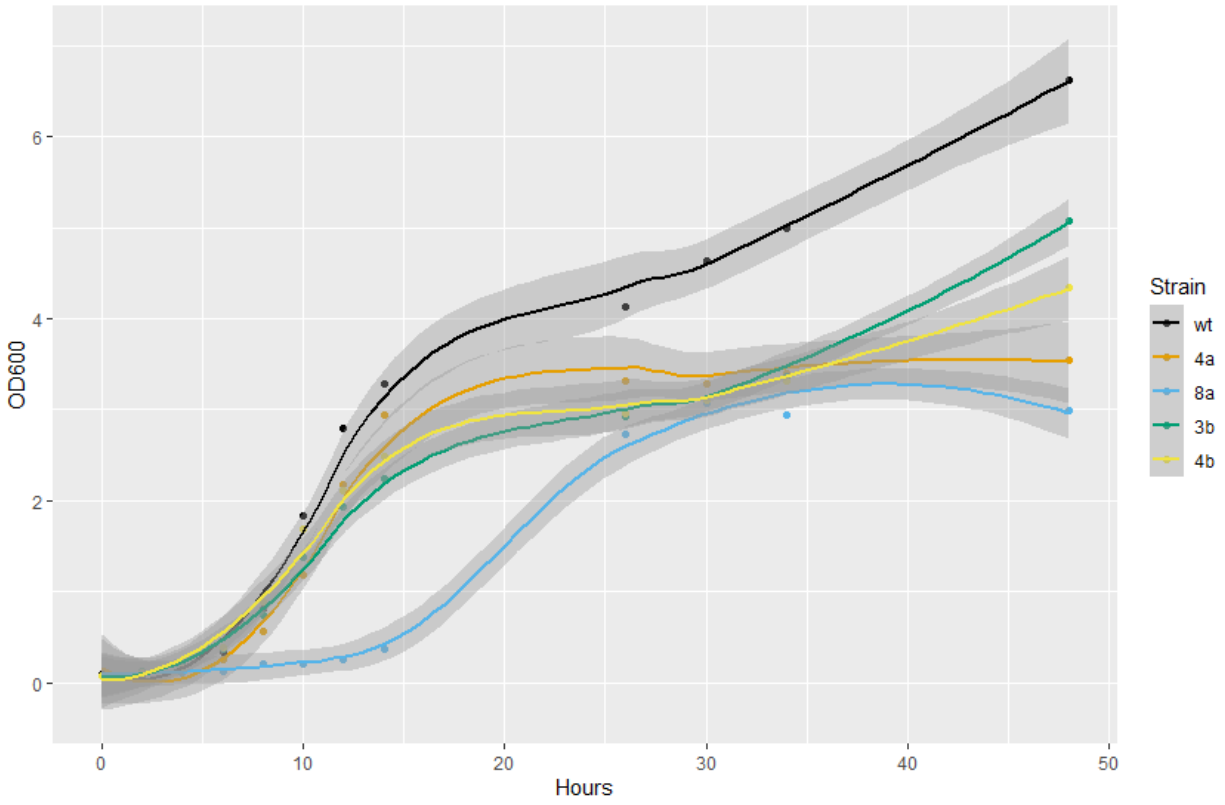

Figure 5. Growth rate comparison between multiple colonies of Ade13-GFP. The growth rate comparison indicated that the earlier Ade13-GFP colony chosen for the growth curve was uniquely defective in growth (see Figure 4) when compared to other individual colonies from the same strain Ade13-GFP strains were grown in YPD continuously at 30ºC with aeration and an aliquot was taken every 2 hours for optical density measurement at 600nm wavelength of light. The OD reading was plotted against time and the growth rate was compared to wild type (B4741) strain.

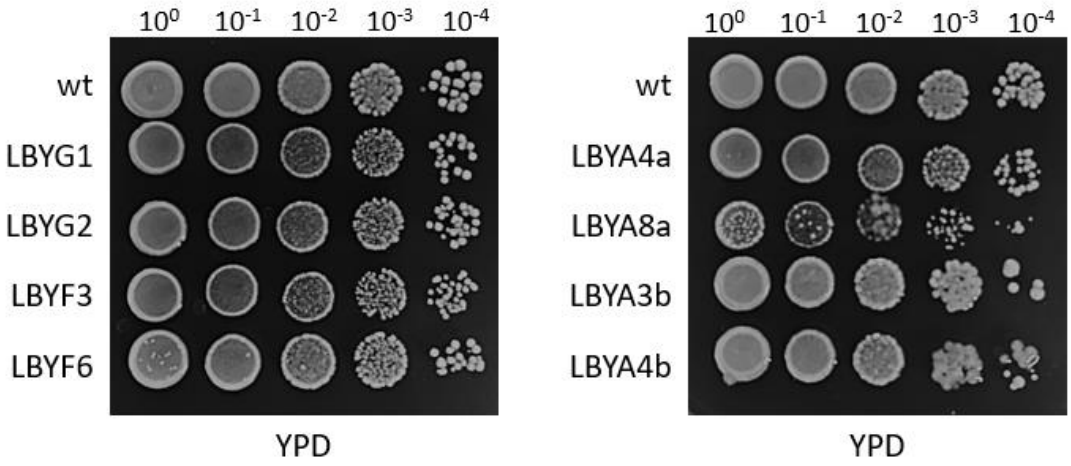

Figure 6. Spotting assay testing the growth of multiple colonies of Ade13 GFP- strains further supports that decreased growth observed earlier is limited to one Ade13 colony (LBYA8a). 10-fold serial dilutions of multiple colonies of Ade13-GFP strain (Table 1) were plated on YPD plates and incubated at 30ºC for 2 days. A wild-type colony (B4741) was also spotted for growth comparison.

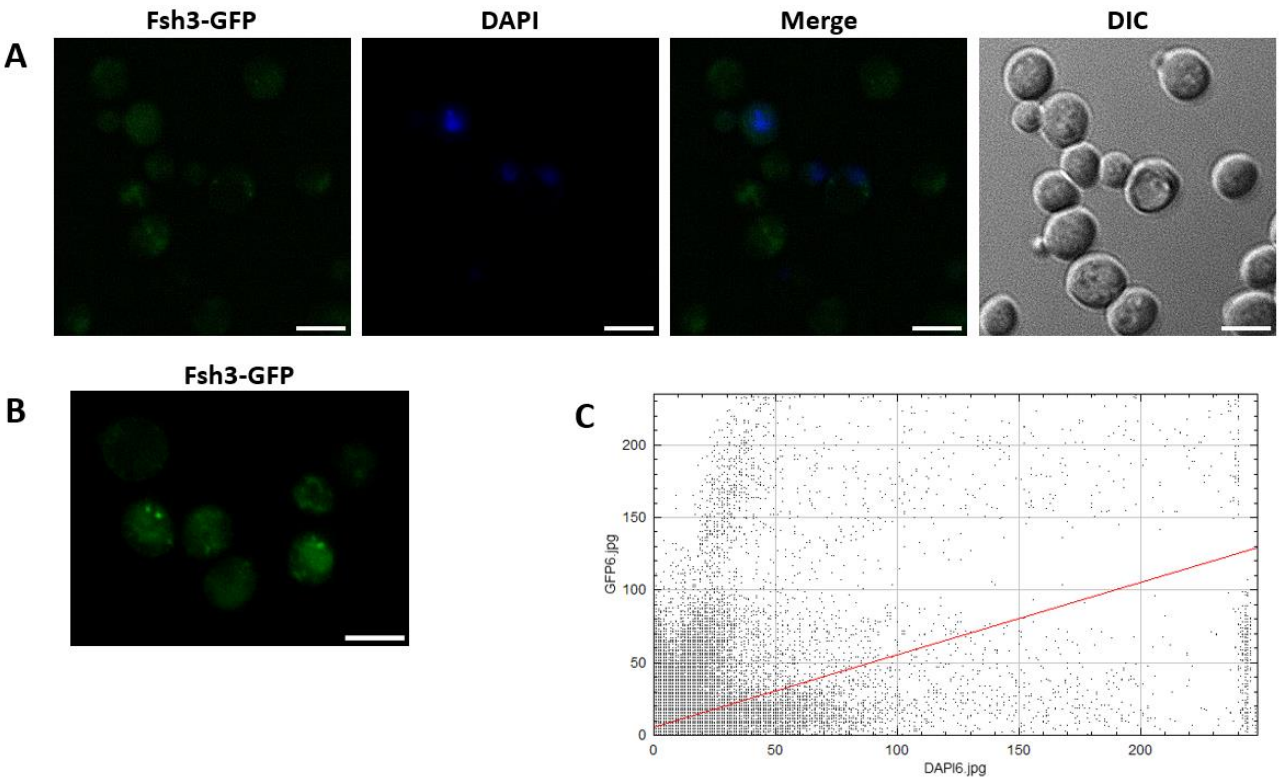

Figure 7. Fluorescence imaging supports that Fsh3-GFP localizes to cytoplasmic puncta. (A) The merged micrographs show distinct puncta that do not colocalize with the nucleus. (B) Additional image depicting cytoplasmic puncta from Fsh3-GFP cells. (C) Cytofluorogram comparing the overlap of fluorescent pixels between DAPI and GFP images. Scale bar = 5µm

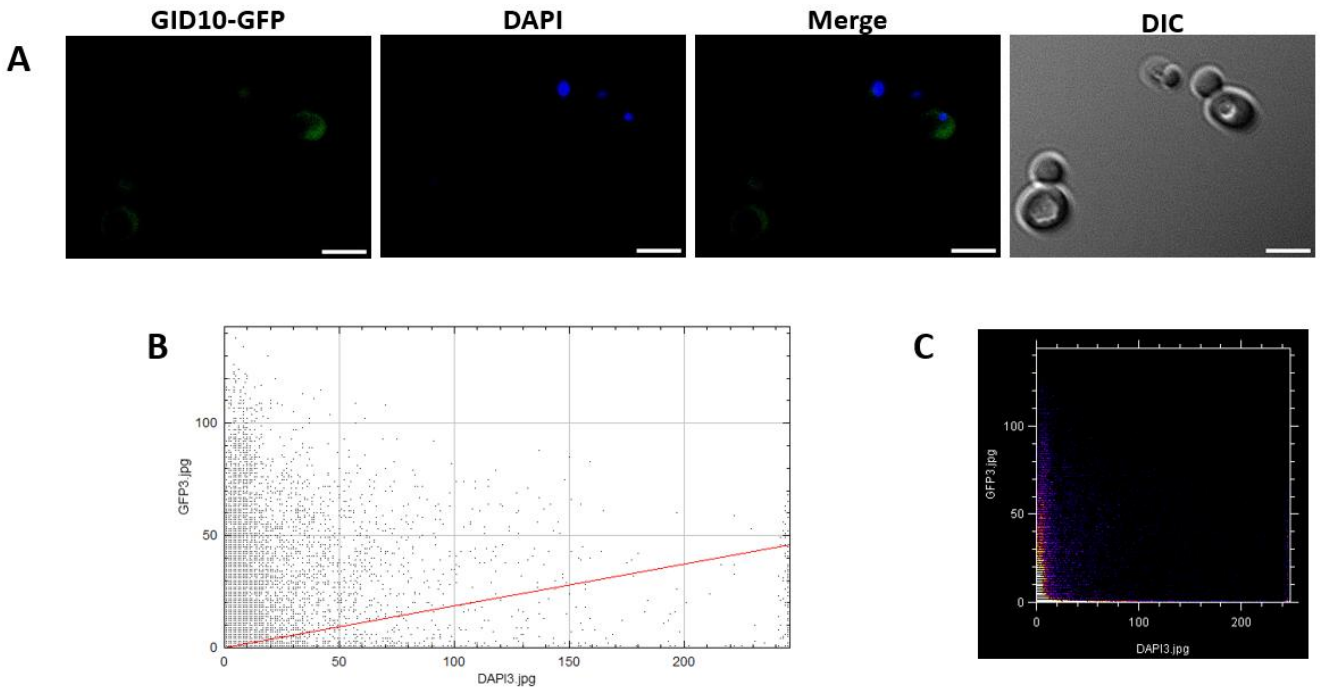

Figure 8. Gid10-GFP is dispersed throughout the cytoplasm. (A) Gid10-GFP cells grown on nutrient-rich media (YPD) show a dispersed pattern of fluorescence throughout the cytoplasm. (B) Cytofluorogram shows a weak correlation between GFP and DAPI fluorescent signals. (C) Pixel fluorogram depicting low similarity between colocalization based on pixel value comparison. Scale bar = 5µm

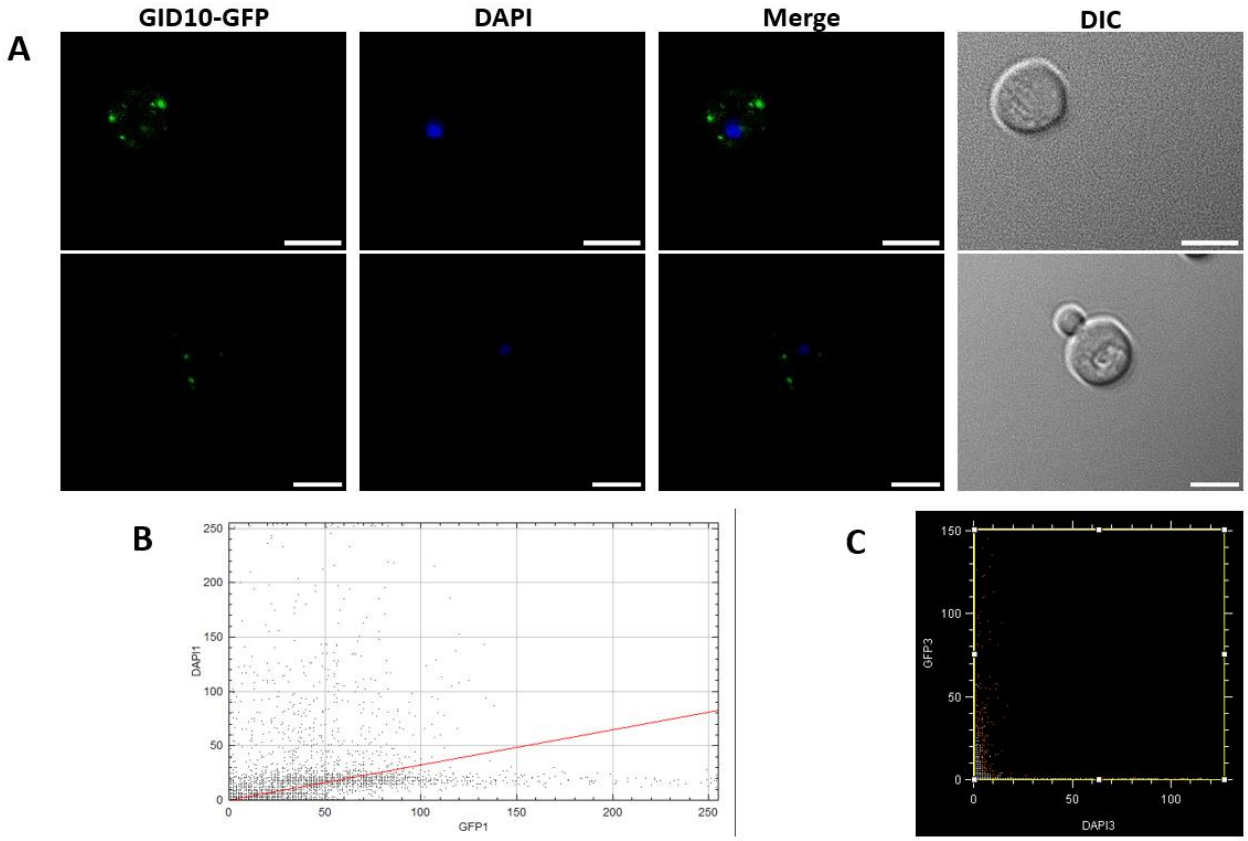

Figure 9. Gid10-GFP localizes to cytoplasmic puncta under glucose-depleting conditions. (A) Gid10-GFP cells grown on media that lacks glucose (YEP) show unique puncta throughout the cytoplasm. (B) Cytofluorogram supports the low correlation between GFP and DAPI fluorescent signals. (C) Pixel fluorogram depicting low similarity between colocalization based on pixel value comparison. Scale bar = 5µm

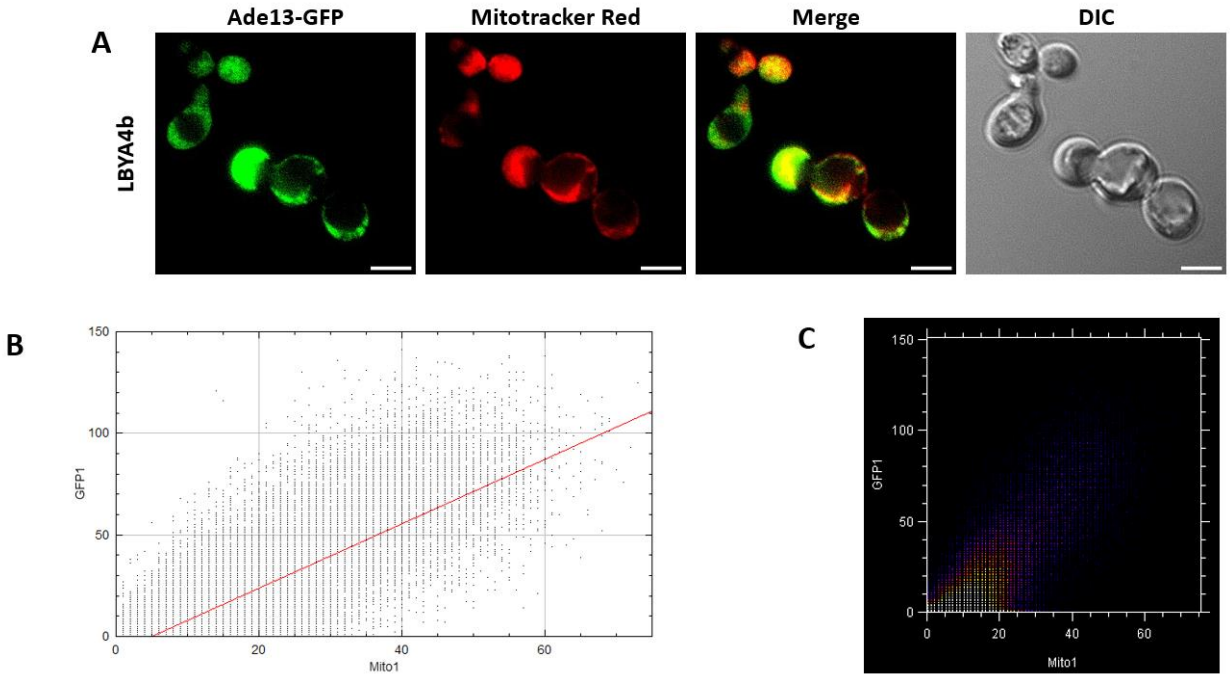

Figure 10. Ade13-GFP localizes to mitochondria. (A) The merged image shows an overlap in Mitotracker Red and GFP, seen in yellow. (B) Cytofluorogram shows a strong correlation between GFP and Mitotracker Red fluorescent signals. (C) Pixel fluorogram depicting higher similarity between colocalization based on pixel value comparison. Scale bar = 5µm

References

Baxter, S.M., Rosenblum, J.S., Knutson, S., Nelson, M.R., Montimurro, J.S., Di Gennaro, J.A., Speir, J.A., Burbaum, J.J., and Fetrow, J.S. (2004). Synergistic computational and experimental proteomics approaches for more accurate detection of serine hydrolases in yeast. *Mol. Cell. Proteomics*, 3(3), 209-215. doi: 10.1074/mcp.M300082-MCP200.

Bolte, S., and Cordelieres, F.P. (2006). A guided tour into subcellular colocalization analysis in light microscopy. *J. Microsc.*, 224, 213-232. doi: 10.1111/j.1365-2818.2006.01706.x.

Camici, M., Micheli, V., Ipata, P.L., and Tozzi, M.G. (2009). Pediatric neurological syndromes and inborn errors of purine metabolism. *Mol. Cell. Neurosci.*, 56, 367-378. doi: 10.1016/j.neuint.2009.12.003.

Chen, S.J., Wu, X., Wadas, B., Oh, J.H., and Varshavsky, A. (2017). An N-end rule pathway that recognizes proline and destroys gluconeogenic enzymes. *Science*, 335(6323), 1-7. doi: 10.1126/science.aal3655.

Cherry, J.M., Adler, C., Ball., Chervitz, S.A., Dwight, S.S., Hester, E.T., Jia, Y., Juvik, G., Roe, T., Schroeder, M., Weng, S., and Botstein, D. (1998). SGD: *Saccharomyces* Genome Database. *Nucleic Acids Res.*, 26(1), 73-79.

Crabtree, H.G. (1929). Observations on the carbohydrate metabolism of tumours. *Biochem. J.* 23, 536-545.

Daignan-Fornier, B., and Pinson, B. (2019). Yeast to study human purine metabolism diseases. *Cells*, 8(1), 67. doi: 10.3390/cells8010067.

De Deken, R.H. (1966) The Crabtree effect: a regulatory system in yeast. *J. Gen. Microbiol*, 44(2), 149-156. doi: 10.1099/00221287-44-2-149.

Denis, V., Boucherie, H., Monribot, C., and Daignan-Fornier, B. (1998). Role of the myb-like proteins bas1p in *Saccharomyces cerevisiae*: a proteome analysis. *Mol. Microbiol.*, 30(3), 557-566. doi: 10.1046/j.1365-2958.1998.01087.x.

Dickinson, J.R, and Schweizer, M. (2004) Metabolism and Molecular Physiology of *Saccharomyces Cerevisiae. CRC Press*, 2. doi: 10.1201/9780203503867.

Dorfman, B.Z. (1969). The isolation of adenylosuccinate synthase mutants in yeast by selection for constitutive behavior in pigmented strains. *Genetics*, 61(2), 377-389. doi: 10.1093/genetics/61.2.377.

Duan, S.F., Han, P.J., Wang, Q.M., Liu, W.Q., Shi, J.Y., Li, K., Zhang, X.L., and Bai, F.Y. (2018). The origin and adaptive evolution of domesticated populations of yeast from far East Asia. *Nat. Commun*, 9, 1-13. doi: 10.1038/s41467-018-05106-7.

Duina, A.A., Miller, M.E., and Keeney, J.B. (2014). Budding yeast for budding genetics: a primer on the *Saccharomyces cerevisiae* model system. *Genetics*, 197(1), 33-48. doi: 10.1534/genetics.114.163188.

Dunn, K.W., Kamocka, M.M., and McDonald, J.H. (2011). A practical guide to evaluating colocalization in biological microscopy. *Am. J. Cell Physial.,* 300, 723-742. doi: 10.1152/ajpcell.00462.2010.

Edgar, R.C. (2004). MUSCLE: multiple sequence alignment with high accuracy and high throughput. *Nucleic. Acids. Res.,* 32(5), 1792-1797. doi: 10.1093/nar/gkh340.

Elsea, S.H, and Girirajan, S. (2008). Smith-Magenis syndrome. *Eur. J. Hum. Genet.,* 16(4), 412-421. doi: 10.1038/sj.ejhg.5202009.

Giaever, G., Chu, A.M., Ni, L., Connelly, C., Riles, L., Veronneau, S., Dow, S., Lucau-Danila, A., Anderson, K., Andre, B., Arkin, A.P., Astromoff, A. Bakkoury, M.E., Bangham, R., Benito, R., Brachat, S., Campanaro, A., Curtiss, M., Davis, K., … Johnston, M. (2002). Functional profiling of the *Saccharomyces cerevisiae* genome. *Nature,* 418, 387-391. doi:

Goffeau, A., Barrell, B.G., Bussey, H., Davis, R.W., Dujon, B., Feldmann, H., Galibert, F., Hoheisel, J.D., Jacq, C., Johnston. M., Louis, E.J., Mewes, H.W., Murakami, Y., Philippsen, P., Tettelin, H., and Oliver, S.G. (1996). Life with 6000 genes. *Science,* 274(5287), 563-564. doi: 10.1126/science.274.5287.546.

Huh, W.K., Falvo, J.V., Gerke, L.C., Carrol, A.S., Howson, R.W., Weissman, J.S., and O'Shea, E.K. (2003). Global analysis of protein localization in budding yeast. *Nature,* 425(6959), 686-691. doi: 10.1038/nature02026.

Jaeken, J., and Van den Berge, G. (1984). An infantile autistic syndrome characterized by the presence of succinylpurines in body fluids. *Lancet.,* 2(8411), 1058-1061.

Jurecka, A., Zikanova, M., Kmoch, S., and Tylki-Szymanska, A. (2015). Adenylosuccinate lyase deficiency. *J. Inherit. Metab. Dis.,* 38(2), 231-242. doi: 10.1007/s10545-014-9755-y

Karathia, H., Vilaprinyo, E., Sorribas, A., and Alves, R. (2011). *Saccharomyces cerevisiae* as a model organism: a comparative study. *PLoS One,* 6(2), e16015. doi: 10.1371/journal.pone.0016015.

Lahue, C., Madden, A.A., Dunn, R.R., and Smukowski Heil, C. (2020). History and domestication of *Saccharomyces cerevisiae* in bread baking. *Front. Genet,* 11, 1-15. doi: 10.3389/fgene.2020.584718.

Larsson, A. (2014) AliView: a fast and lightweight alignment viewer and editor for large data sets. *Bioinformatics,* 30(22), 3276-3278.

Lenburg, M.E., and O'Shea, E.K. (1996). Signaling phosphate starvation. *Trends Biochem. Sci.,* 21(10), 383-387.

Liti, G. (2015). The natural history of model organisms: the fascinating and secret wild life of the budding yeast *S. cerevisiae. eLife,* 4, 1-9. doi: 10.7554/eLife.05835.

Longtine, M.S., McKenzie 3rd, A., Demarini, D.J., Shah, N.G., Wach, A., Brachat, A., Philippsen, P., and Pringle, J.R. (1998). Additional modules for versatile and economical PCR-based gene deletion and modification in *Saccharomyces cerevisiae. Yeast.,* 14(10), 953-961. doi: 10.1002/(SICI)1097-0061(199807)14:10<953::AID-YEA293>3.0.CO;2-U.

Madeira, F., Pearce, M., Tivey, A.R.N., Basutkar, P., Lee, J., Edbali, O., Madhusoodanan, N., Kolesnikov, A., Lopez, R. (2022). Search and sequence analysis tools service from EMBL-EBI in 2022. *Nucleic Acids. Res.,* 50(1), 276-279. doi. 10.1093/nar/gkac240.

Melnykov, A., Chen, S.J., and Varshavsky, A. (2019). Gid10 as an alternative N-recognition of the Pro/N-degron pathway. *Proc. Natl. Acad. Sci. USA,* 116(32), 15914-15923. doi: 10.1073/pnas.1908304116.

Mortimer, R.K., and Johnston, J.R. (1986). Genealogy of principle strains of the yeast genetic stock center. *Genetics,* 113(1), 35-43. doi: 10.1093/genetics/113.1.35.

Notzel, C., Linger, T., Klingenberg, H., and Thoms, S. (2016). Identification of new fungal peroxisomal matrix proteins and revision of the PTS1 consensus. *Traffic,* 17(10), 1110-1124. doi: 10.1111/tra.12426.

Phillips, N., Zeigler, M., Saha, B., and Xynos, F. (1993). Allelic loss on chromosome 17 in human ovarian cancer. *Int. J. Cancer,* 54, 85-91.

Potocki, L., Bi, W., Treadwell-Deering, D., Carvalho, C.M.B., Eifert, A., … Lupski, J.R. (2007). Characterization of Potocki-Lupski syndrome (dup(17)(p11.2p11.2)) and delineation of a dosage-sensitive critical interval that can convey an autism phenotype. *Am. J. Hum. Genet.,* 80(4), 633-649. doi: 10.1086/512864.

Regelmann, J., Schule, T., Josupeit, F.S., Horak, J., Rose, M., Entian, K.D., Thumm, M., and Wolf, D.H. (2003). Catabolic degradation of fructose-1,6-biphosphate in the yeast *Saccharomyces cerevisiae:* A genome-wide screen identifies eight novel *GID* genes and indicates the existence of two degradation pathways. *Mol. Biol. Cell.,* 14(4), 1652-1663. doi: 10.1091/mbc.E02-08-0456.

Revell, L.J. (2011). Phytools: an R package for phylogenetic comparative biology (and other things). *Methods Ecol. Evol.,* 3(2), 217-223. doi: 10.1111/j.2041-210X.2011.00169.x.

Schneider, C.A., Rasband, W.S., and Eliceiri, K.W. (2012). NIH image to ImageJ: 25 years of image analysis. *Nat. Methods,* 9, 671-675. doi: 10.1038/nmeth.2089.

Sopko, R., Huang, D., Preston, N., Chua, G., Papp, B., Kafadar, K., Snyder, M., Oliver, S.G., Cyert, M., Hughes, T.R., Boone, C., and Andrews, B. (2006). Mapping pathways and phenotypes by systemic gene overexpression. *Mol. Cell.,* 21(3), 319-330. doi: 10.1016/j.molcel.2005.12.011.

Varshavsky, A. (2019). N-degron and C-degron pathways of protein degradation. *Proc. Natl. Acad. Sci. USA,* 116(2), 358-366. doi: 10.1073/pnas.1816596116.

Wisecaver, J.H., Slot, J.C., and Rokas, A. (2014). The evolution of fungal metabolic pathways. *PLoS Genet.,* 10(12), e1004816. doi: 10.1371/journal.pgen.1004816.

Wainright, M. (1988). Metabolic diversity of fungi in relation to growth and mineral cycling in soil – a review. *Trans. Br. Mycol. Soc*, 90(2), 159-170. doi: 10.1016/S0007-1536(88)80084-0.

Yifrach, E., Holbrook-Smith, D., Burgi, J., Othman, A., Eisenstein, M., WT van Roermund, C., Visser, W., Tirosh, A., Rudowitz, M., Bibi, C., Galor, S., Weill, U., Fadel, A., Peleg, Y., Erdmann, R., Waterham, H.R., Wanders, R.J.A., Wilmanns, M., Zamboni, N., Schuldiner, M., and Zalckvar, E. (2022). Systematic multi-level analysis of an organelle proteome reveals new peroxisomal functions. *Mol. Syst. Biol.,* 18(9), e11186. doi: 10.15252/msb.202211186

Yofe, I., and Schuldiner, M. (2014). Primers-4-Yeast: a comprehensive web tool for planning primers for *Saccharomyces cerevisiae. Yeast.,* 31(2), 77-80.